

OPEN

A ribosomal protein S5 isoform is essential for oogenesis and interacts with distinct RNAs in *Drosophila melanogaster*

Jian Kong¹, Hong Han¹, Julie Bergalet², Louis Philip Benoit Bouvrette^{2,3}, Greco Hernández^{1,5}, Nam-Sung Moon¹, Hojatollah Vali⁴, Éric Lécuyer² & Paul Lasko¹ 

In *Drosophila melanogaster* there are two genes encoding ribosomal protein S5, *RpS5a* and *RpS5b*. Here, we demonstrate that *RpS5b* is required for oogenesis. Females lacking *RpS5b* produce ovaries with numerous developmental defects that undergo widespread apoptosis in mid-oogenesis. Females lacking germline *RpS5a* are fully fertile, but germline expression of interfering RNA targeting germline *RpS5a* in an *RpS5b* mutant background worsened the *RpS5b* phenotype and blocked oogenesis before egg chambers form. A broad spectrum of mRNAs co-purified in immunoprecipitations with *RpS5a*, while *RpS5b*-associated mRNAs were specifically enriched for GO terms related to mitochondrial electron transport and cellular metabolic processes. Consistent with this, *RpS5b* mitochondrial fractions are depleted for proteins linked to oxidative phosphorylation and mitochondrial respiration, and *RpS5b* mitochondria tended to form large clusters and had more heterogeneous morphology than those from controls. We conclude that *RpS5b*-containing ribosomes preferentially associate with particular mRNAs and serve an essential function in oogenesis.

Increasing evidence indicates that ribosomes are heterogeneous and perhaps dynamic, in contrast to the classical view of them as constitutive machinery for protein synthesis^{1–11}. In *Drosophila melanogaster*, nine ribosomal protein genes are each present in two paralogs, and in many of these cases one of the paralogs is primarily expressed in germline tissues^{12–14}. Single paralogs of four genes encoding ribosomal proteins (*RpS5b*, *RpS10a*, *RpS19b*, and *RpL22-like*) are abundantly expressed in germline stem cells and primordial germ cells^{15,16}. *RpS5b* is also upregulated in *l(3)mbt* brain tumors whose cells are in an undifferentiated state and express many germline-specific genes, of which some have been implicated in tumor growth¹⁷. These observations suggest that variant ribosomes with different protein composition may be an important factor in establishing or maintaining stem cell and/or germline identity. To investigate this and to explore the role of a variant ribosomal protein in metazoan development, we examined the cellular and developmental functions of *Drosophila melanogaster* *RpS5b*.

Results

Different forms of ribosomal protein S5 are encoded by two different genes and expressed in complementary patterns. *D. melanogaster* *RpS5a* and *RpS5b* have distinct N-terminal domains of approximately 40 amino acids in length, while the remainders of the two proteins are nearly identical. The N-terminal domains of *D. melanogaster* *RpS5a* and *RpS5b* are not conserved in *RpS5* orthologues in *C. elegans* or yeast, and the single mammalian form of *RpS5* is a shorter protein that lacks the divergent N-terminal domain (Fig. 1a). Using paralog-specific antisera that respectively recognize N-terminal peptides of *RpS5a* and *RpS5b*, we determined that both paralogs are incorporated into ribosomes, since they co-purify with a canonical ribosomal protein, *RpS6* (Fig. 1b). *RpS5b* migrates on sucrose gradients in a similar manner to *RpS5a*, with major peaks

¹Department of Biology, McGill University, 3649 Promenade Sir William Osler, Montréal, QC, H3G 0B1, Canada.

²Montreal Clinical Research Institute (IRCM), 110 Avenue des Pins Ouest, Montréal, QC, H2W 1R7, Canada.

³Département de Biochimie, Université de Montréal, Montréal, QC, H3C 3J7, Canada. ⁴Facility for Electron Microscopy Research, Faculty of Dentistry, McGill University, Montréal, QC, Canada. ⁵Present address: Unit of Biomedical Research on Cancer, National Institute of Cancer, Tlalpan, 14080, Mexico City, Mexico. Correspondence and requests for materials should be addressed to P.L. (email: paul.lasko@mcgill.ca)

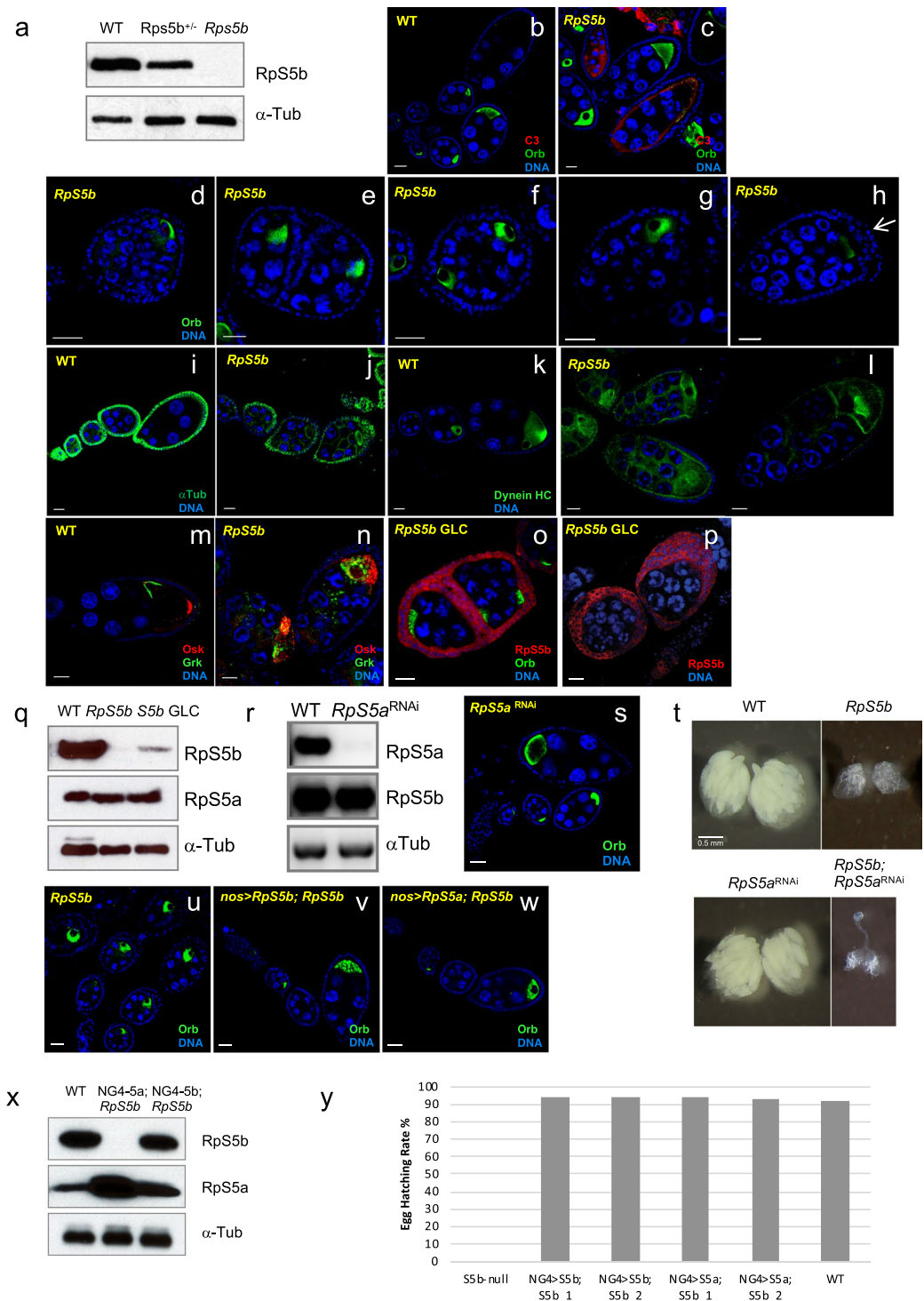


Figure 2. *RpS5b* mutant ovaries have numerous developmental defects that can be rescued by germline expression of *RpS5a* or *RpS5b*. **(a)** Western blot demonstrating that RpS5b is undetectable in *RpS5b* homozygotes and present at reduced levels in *RpS5b* heterozygotes, confirming the loss-of-function nature of the mutation. **(b,c)** Oogenesis does not proceed beyond stage 8 in *RpS5b* ovaries, at which point apoptosis is induced, as measured by increased levels of activated caspase-3 (C3). α-Orb is used to label the oocyte. **(d–h)** Various defects observed in *RpS5b* ovaries: **(d)** an extra round of germ cell division; **(e)** a compound egg chamber partially separated by follicle cells, **(f)** oocyte duplication in a single egg chamber; **(g)** mis-localized oocyte; **(h)** multiple layers of follicle cells at the posterior of the egg chamber (white arrow). **(i–l)** Alterations in the microtubule cytoskeleton in *RpS5b* oocytes, as measured by immunostaining against **(i,j)** α-Tubulin, or **(k,l)** α-Dynein heavy chain. Note the aberrant accumulation of α-Tubulin around the oocyte in **(j)**, and the focus of Dynein in the centre of the oocyte in **(l)**. **(m,n)** Distribution of Osk and Grk in **(m)** wildtype and **(n)** *RpS5b* oocytes, showing that deployment of these proteins is disrupted in the mutant. **(o,p)** Analysis of *RpS5b* germline clones, showing similar defects as found in the mutant, but more extreme overproliferation of follicle

cells. **(q)** Western blot showing RpS5b expression in *RpS5b* mutant and germline clones. The residual expression in the germline clones is somatic, as is also apparent in **(o,p)**. **(r)** Western blot comparing RpS5a expression in 0–2 h embryos collected from wildtype females and those expressing shRNA targeting *RpS5a* driven by the germline-specific promoter *nos*, showing the efficacy of knockdown. **(s)** Analysis of ovaries from females expressing shRNA targeting RpS5a driven by the germline-specific promoter *nos*, showing normal patterning. **(t)** Brightfield images of whole ovaries showing that *RpS5a* germline knockdown produces no phenotype but worsens the *RpS5b* mutant phenotype. **(u–w)** *RpS5b* mutant ovaries **(u)** without a transgene as control or expressing transgenic **(v)** *RpS5b* or **(w)** *RpS5a* under the control of the *nos* promoter. Normal oogenesis is restored in both cases. **(x)** Western blot of lysates from 0–2 h embryos collected from wildtype (WT), *nos > RpS5a*; *RpS5b* (NG4–5a; *S5b*) and *nos > RpS5b*; *RpS5b* (NG4–5b; *S5b*) females, confirming high-level expression from the transgenes. **(y)** Graph showing hatching rates of embryos from females of the genotypes indicated, demonstrating that either *RpS5a* or *RpS5b* can fully rescue the fertility of *RpS5b* females when expressed in germline.

examine the consequences of loss of RpS5b, we obtained an *RpS5b* mutant from a large-scale insertion mutagenesis screen (*RpS5b*^{G5346})¹⁹, subsequently referred to simply as *RpS5b*, that does not produce detectable levels of protein, as assessed by immunoblotting from ovaries (Fig. 2a). *RpS5b* mutant flies are fully viable and male *RpS5b* mutant flies are fertile. Female *RpS5b* mutant flies, however, are completely sterile and do not complete oogenesis. The nurse cells, follicle cells, and oocyte of these flies all differentiate, but very few egg chambers progress beyond stage 8–9, after which point apoptosis is induced, as measured by cleaved caspase-3 immunostaining (Fig. 2b,c). In addition, we observed numerous developmental defects in *RpS5b* mutant ovaries. Some egg chambers contained more than 16 germ cells with one or two oocytes (Fig. 2d, Supplementary Fig. S2a, 0.8% and 6.4% respectively in 975 stage 4 and later egg chambers examined by light microscopy), some egg chambers failed to separate (Fig. 2e, 8.1% out of 975 egg chambers examined by light microscopy), while others had 16 germ cells but two oocytes (Fig. 2f, 1.1% out of 975) or a mis-localized oocyte (Fig. 2g, 2.9% out of 975). We also frequently observed over-proliferation of follicle cells with multiple cell layers present at the posterior of egg chambers (Fig. 2h, 54% out of 341 examined by confocal microscopy). Polarity defects in *RpS5b* mutant oocytes were also observed. Immunostaining for α -Tubulin and for Dynein heavy chain, which marks the microtubule organizing center normally present at the posterior of the stage 7 oocyte, revealed that microtubules were improperly aligned, often accumulating near the anterior of *RpS5b* mutant oocytes (Fig. 2i–l). Consistent with this, spatial targeting of Oskar and Gurken, both microtubule-dependent processes, was disturbed in all stage 8 and later *RpS5b* oocytes that were examined (Fig. 2m,n). Phalloidin staining revealed an overabundance of F-actin in *RpS5b* oocytes (Supplementary Fig. S2b,c).

Overlapping functions for RpS5a and RpS5b. Since *RpS5b* is primarily expressed in germline cells, we were surprised to observe phenotypes in the mutant that affected follicle cells as well as the germline. To analyze the requirement for *RpS5b* in the germline specifically, we used the dominant female sterile-FLP technique²⁰ to produce flies that lacked *RpS5b* function only in germline cells. Ovaries from *RpS5b* germline clone flies exhibited the same set of phenotypes, often with even greater severity, as the mutant flies (Fig. 2o,p). In particular, many egg chambers had multiple layers of follicle cells, and encapsulation defects were observed. We confirmed that these extra cells were follicle staining by immunostaining for Cut protein (Supplementary Fig. S3), which is expressed in mitotic follicle cells²¹. As measured by immunostaining (Fig. 2o,p) and immunoblotting (Fig. 2q), these flies produce very little RpS5b, strictly from somatic expression, which can be visualized in follicle cells using confocal microscopy with increased gain. Next, to investigate whether RpS5a functions in the germline, we drove expression of a short hairpin RNA that targets it in germline cells, which drastically reduced accumulation of the protein in early-stage progeny embryos (Fig. 2r). Females lacking germline RpS5a were fertile and proceeded through oogenesis normally, and produced progeny (Fig. 2s,t). However, knocking down germline expression of RpS5a in an *RpS5b* mutant background gave a much more severe phenotype than the *RpS5b* mutant presents on its own; in this case flies possess only very rudimentary ovaries and no formation of egg chambers is apparent (Fig. 2t). We conclude from these observations that both RpS5a and RpS5b function in germline in normal development, but also that germline RpS5b can functionally substitute for germline RpS5a.

We wanted to distinguish whether the failure of endogenous germline RpS5a to functionally substitute for RpS5b in the *RpS5b* mutant was due to functional differences between the two proteins, or whether there is insufficient endogenous expression of RpS5a in germline to rescue the function of RpS5b. To do this, we expressed both untagged and N-terminally tagged forms of RpS5a and RpS5b with *nos*, a germline specific promoter, and examined whether fertility could be restored to the *RpS5b* mutant. We observed that *nos*-driven expression of either RpS5a or RpS5b, in either untagged or Venus-tagged forms, indeed restored normal oogenesis and full fertility to the *RpS5b* mutant (Fig. 2u–y, Supplementary Fig. S2d–i'). We conclude that RpS5a can substitute for RpS5b in germline tissue provided it is expressed at high enough levels.

High-throughput analysis reveals that RpS5b associates preferentially with nuclear-encoded mRNAs involved in mitochondrial processes. As we have demonstrated, the endogenous forms of RpS5a and RpS5b are primarily expressed in different cell types, so for this reason it is very likely that they associate with different RNA populations in normal development. To investigate whether they preferentially associate with particular mRNAs when present in the same tissue, we expressed FLAG-HA-RpS5a (FH-RpS5a) or FLAG-HA-RpS5b (FH-RpS5b) in the germline using *nos > Gal4*, and then co-immunoprecipitated (co-IP) the associated RNAs with anti-FLAG antibody. We identified a set of transcripts that were enriched in FH-RpS5b

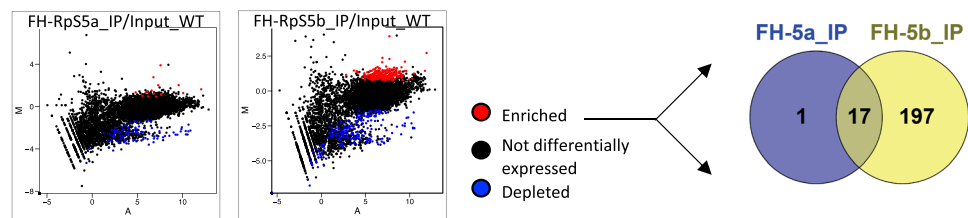
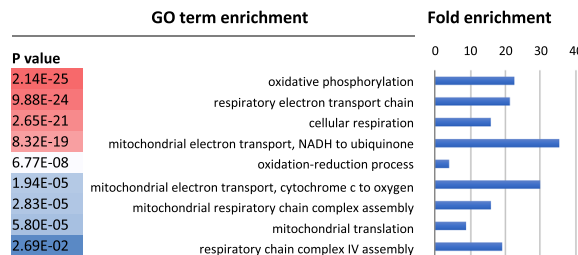
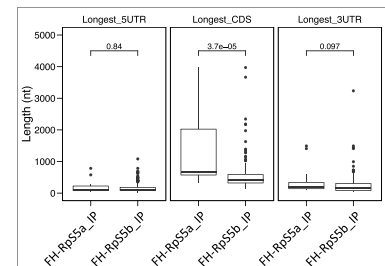
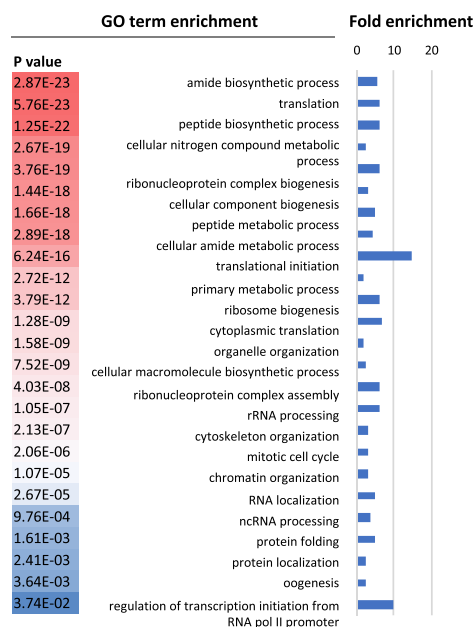
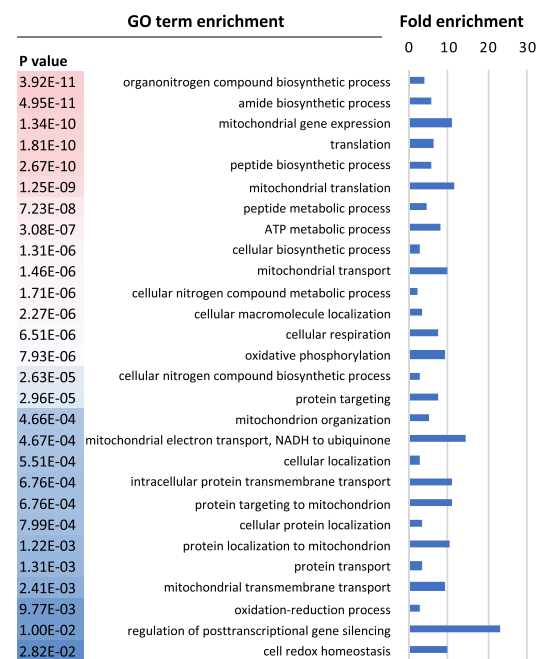
a RIPseq: FH-RpS5a vs FH-RpS5b**b** RIPseq: FH-RpS5b exclusive enrichment**c****d** MS: enriched in *RpS5b* mitochondria**e** MS: depleted in *RpS5b* mitochondria

Figure 3. Analysis of RNA populations recruited by FLAG-HA (FH)-RpS5a and RpS5b. **(a)** MA plot of RNA immunoprecipitations from the ovaries with germline overexpression of either FH-RpS5a or FH-RpS5b in the wildtype background with α -FLAG compared to input. Statistically enriched (>2 fold, $\text{padj} < 0.01$) and depleted (<2 fold, $\text{padj} < 0.01$) are highlighted in red and blue respectively. $M = \log_2(\text{pulldown}) - \log_2(\text{input})$, $A = 0.5 * (\log_2(\text{pulldown}) + \log_2(\text{input}))$. Fold changes and adjusted p-values (padj) calculated by DESeq2³⁸. The Venn diagram (<http://bioinfogp.cnb.csic.es/tools/venny/>) shows limited overlap between RNAs enriched in populations recruited by FH-RpS5a (FH-5a) and RpS5b (FH-5b). **(b,c)** Heat map representing biological process gene ontology (GO) terms of RNAs enriched in populations recruited by **(b)** FH-RpS5b (Statistical overrepresentation test on Pantherdb.org). The most highly significant matches are in red. The fold enrichment of each GO term is plotted in the bar chart. **(c)** Box plot of the length distribution, in nucleotides, of the 5'UTR, coding sequence (CDS) and 3'UTR for RNAs enriched in populations recruited by FH-RpS5a (FH-RpS5a_IP) and FH-RpS5b (FH-RpS5b_IP). **(d,e)** Heat maps representing the biological process GO terms associated with the proteins **(d)** enriched or **(e)** depleted in the mitochondrial fractions from *RpS5b* ovaries as compared with wild-type. The most highly significant matches are in red³⁹.

co-IPs in comparison to input (Fig. 3a). Gene ontology (GO) term analysis revealed that FH-RpS5b-associated mRNAs are most highly enriched for those involved in oxidative phosphorylation, electron transport chain function, electron transport chain assembly and mitochondrial translation (Fig. 3b and Supplementary Table S1). Far fewer mRNAs were preferentially recovered in FH-RpS5a co-IPs (Fig. 3a), and no GO terms were significantly enriched among them. mRNAs enriched in FH-RpS5b co-IPs generally had very short coding regions (CDS) that were significantly different from those that associate with FH-RpS5a (Fig. 3c). Taken together, these data support that there is selectivity between RpS5a and RpS5b as to the mRNAs they recruit.

We also conducted similar co-immunoprecipitation experiments and RNA sequencing with wildtype ovaries using antisera that recognize each of the RpS5 paralogs, in order to determine whether these binding preferences are also observed in normal development. Again, largely non-overlapping sets of transcripts were enriched in either the RpS5a or RpS5b immunoprecipitates in comparison to input (Supplementary Fig. S4a). GO term analysis again revealed that RpS5b-associated mRNAs are most highly enriched for those involved in oxidative phosphorylation, electron transport chain function, electron transport chain assembly, and mitochondrial translation (Supplementary Fig. S4b and Table S2), and many RpS5b-associated mRNAs encode proteins that localize to the mitochondrial inner membrane. In contrast, only high-level GO terms related to transcriptional regulation, development, and morphogenesis were enriched among RpS5a-associated mRNAs (Supplementary Fig. S4b).

In addition to functional differences, we also found structural differences in the populations of RNAs that associate with RpS5a and RpS5b. RpS5b-associated mRNAs were smaller, again with significantly shorter CDS, but also with significantly shorter 5' and 3' UTRs, than RpS5a-associated mRNAs (Supplementary Fig. S4c). We also identified sequence motifs that were selectively enriched within RpS5b- or RpS5a-associated mRNA targets (Supplementary Fig. S4d). While these motifs have no established function, their differential enrichment provides further evidence that RpS5a and RpS5b preferentially associate with different populations of mRNAs.

To investigate whether RpS5a can be recruited to mRNAs that are normally associated with RpS5b, we examined the population of RpS5a-associated mRNAs in the *RpS5b* mutant. In this situation, the average 5' UTR and 3' UTR lengths of RpS5a-associated mRNAs were significantly shorter than those of RpS5a-associated mRNAs in the ovary with wildtype RpS5b, but significantly longer than those of RpS5b-associated mRNAs in the ovary with wildtype RpS5b (Supplementary Fig. S4c). We then individually examined the 62 mRNAs that were most enriched to RpS5b in wildtype and compared their association with RpS5a in wildtype and *RpS5b* background. We found that most of them were associated to RpS5a to an elevated degree in the *RpS5b* mutant (Supplementary Fig. S4e). Importantly, GO terms related to oxidative phosphorylation and mitochondrial processes were not significantly enriched among RpS5a-associated mRNAs in the *RpS5b* mutant. These results suggest that germline RpS5a can to some extent recruit mRNAs that normally associate with RpS5b when RpS5b is absent in the *RpS5b* mutant, but that this compensation is only partial and insufficient to rescue oogenesis, leading to the phenotypes we observe.

Proteomic analysis reveals depletion of mitochondria proteins in *RpS5b* ovaries. To investigate the role of RpS5b in global translation, we used tandem mass spectrometry to compare the proteomes of similarly staged *RpS5b* and wildtype ovaries. We prepared lysates from these tissues and separated them into cytosolic and mitochondrial fractions by centrifugation. The levels of many proteins changed significantly in *RpS5b* lysates versus wildtype. We observed enrichment of some classes of proteins in the mitochondrial fraction of *RpS5b* lysates, notably those involved in translation and other RNA dependent processes (Fig. 3d and Supplementary Table S3). This does not necessarily imply increased levels of these proteins, as increased association of the cytosolic translational machinery with the mitochondrial outer membrane to support mitochondrial biogenesis during *Drosophila* oogenesis has been previously described²². Consistent with the RNA analysis, proteins with GO terms related to oxidative phosphorylation were depleted in the *RpS5b* mitochondrial fraction as compared to wildtype (Fig. 3e and Supplementary Table S3). Proteins with higher abundance in the cytosol of *RpS5b* ovaries fell into numerous categories, while those with lower abundance included those involved in developmental processes that occur in later oogenesis, reflecting the developmental block during oogenesis in these ovaries (Supplementary Fig. S5).

***RpS5b* mitochondria have altered morphology and form large aggregates.** Since our analysis indicated particular effects on mitochondrial components, we examined the morphology and function of mitochondria in *RpS5b*-null ovaries. Immunostaining of mitochondria in the mutant ovary showed extensive clustering, in contrast to the more dispersed distribution of mitochondria in wildtype (Fig. 4a). This pattern was confirmed in the *RpS5b* germline clones (Fig. 4a), indicating that the mitochondrial phenotype is due to the lack of germline RpS5b.

To further investigate this, we employed transmission electron microscopy (TEM) and focus ion beam scanning electron microscopy (FIB-SEM) to image the mitochondria in nurse cells of both wildtype and *RpS5b* ovaries. Again, the mitochondria in the *RpS5b* ovary appeared to form extensive clusters (Supplementary Fig. S6a). In most cases, *RpS5b* mitochondria were less elongated and had less well resolved cristae (Fig. 4b,c). Sometimes two *RpS5b* mitochondria adhere to each other via the outer membrane (Fig. 4b), and some *RpS5b* mitochondria bend and engulf some cytoplasm, forming a donut shape. These patterns were observed both in *RpS5b* mutant and germline clones (Fig. 4b). To further analyze the structure of *RpS5b* mitochondria, focused ion beam-scanning electron microscopy (FIB-SEM) of 120 consecutive serial sections of 4 nm thickness was performed. Reconstructed data produced in this way revealed the 3D structure of the donut-shape mitochondria as engulfing cytosolic material (Supplementary Fig. S6b, movie showing z-stack). To test whether loss of RpS5b affects mitochondrial function *in vivo*, we treated live ovaries with CellROX, a reagent that measures reactive oxygen species (ROS) levels. We observed markedly elevated ROS levels in *RpS5b* mutant ovaries, consistent with mitochondrial dysfunction (Fig. 4d).

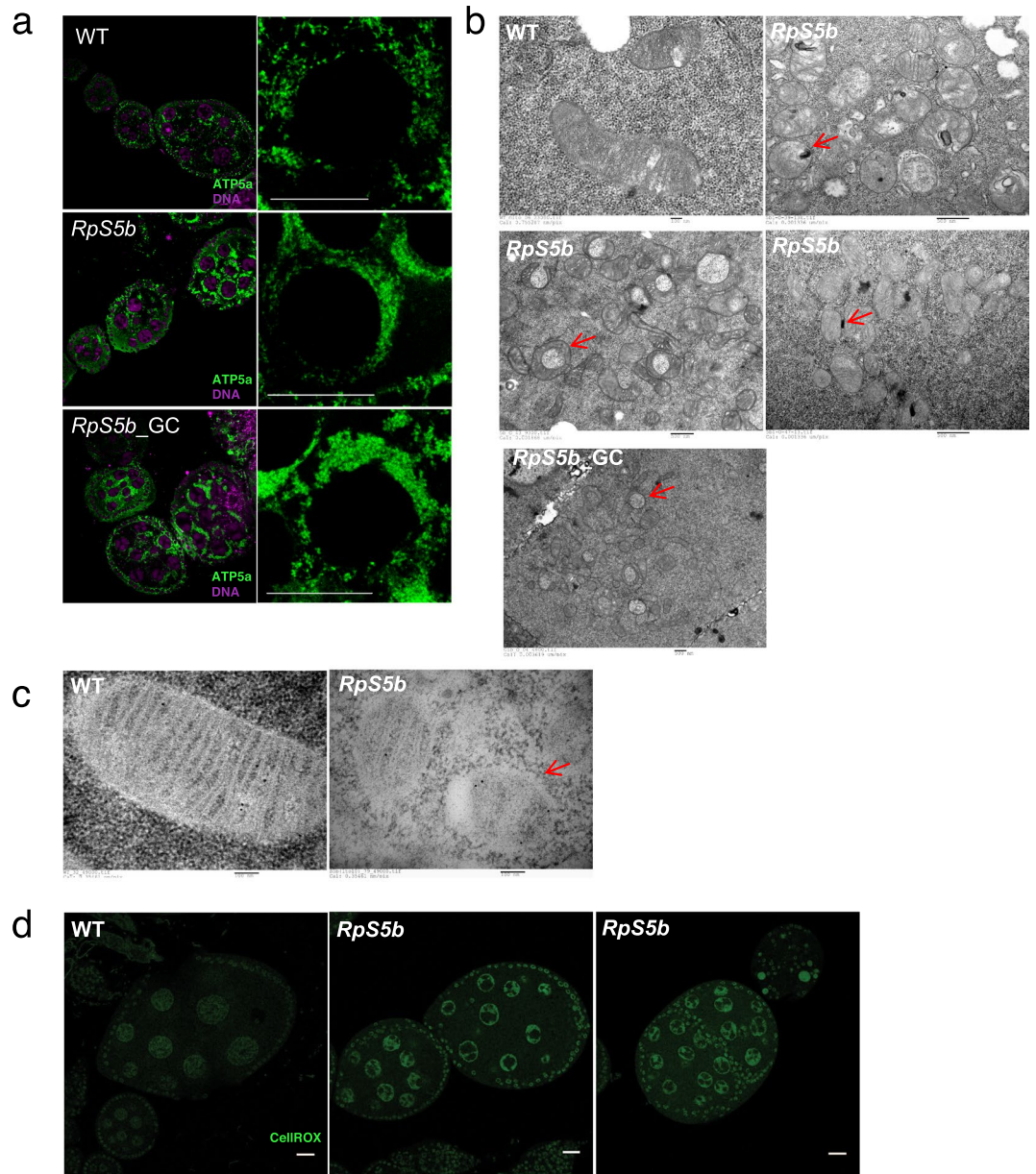


Figure 4. *RpS5b* ovaries have mitochondria with aberrant distribution and morphology, and elevated ROS. (a) Immunostaining for α -ATP5a, a subunit of mitochondrial ATP synthase, reveals a much more densely clustered distribution of mitochondria in nurse cells from *RpS5b*, or *RpS5b* germline clones (*RpS5b_GC*) than from wildtype (WT). (b) Transmission electron micrographs (TEM) of thin sections from nurse cells show that *RpS5b* mutant or *RpS5b* germline clones have mitochondria with aberrant cristae morphology and irregular shapes (red arrows). (c) TEM images of mitochondria labeled with colloidal-gold conjugated α -ATP5a, illustrating morphological changes in *RpS5b* mitochondria (red arrow). (d) Images of live ovaries from wildtype (WT) and *RpS5b* females treated with CellROX, a sensor for reactive oxygen species (ROS), showing elevated levels in *RpS5b*.

Discussion

Our experiments demonstrate that *RpS5b*, one of two *RpS5* paralogs in *Drosophila*, is required for completion of oogenesis and for female fertility. While *RpS5a* is primarily expressed in somatic cells and *RpS5b* is primarily expressed in germline, we present genetic evidence that both paralogs function in germline in early stages of oogenesis, as germline-specific knockdown of *RpS5a* exacerbates the *RpS5b* phenotype, producing a very early arrest in oogenesis. There is other evidence that non-canonical components of the translational machinery is required in pluripotent cells. For example, two forms of eukaryotic initiation factor 4G (eIF4G) are expressed in *Drosophila* testes. In a situation analogous to *RpS5a* and *RpS5b*, eIF4G is primarily expressed in soma and eIF4G2 is primarily expressed in germline, but germline specific knockdown of both eIF4G and eIF4G2 produces a more severe phenotype than germline specific knockdown of eIF4G2 alone²³. Another example is in *Drosophila* oogenesis, where MexTli, a protein related to eIF4G, is expressed specifically in germline stem cells and early-stage

cystocytes, where it binds eIF4E and promotes translation²⁴. It is also noteworthy that, while most mammalian ribosomal proteins exist only in one form, an exception is RpS4, which is encoded by three genes, one on the X and two on the Y chromosome, with one of the Y-linked genes primarily expressed during spermatogenesis²⁵. Taken together, these results indicate that germline cells rely upon a specialized translational machinery.

We further demonstrate that ribosomes containing RpS5a and RpS5b associate with distinct populations of RNAs. Most notably, RpS5b-associated mRNAs are highly enriched for those encoding mitochondrial proteins involved in oxidative phosphorylation. Consistently, this class of proteins is depleted in *RpS5b* ovaries, which also exhibit abnormalities in mitochondrial distribution and morphology. Rapid growth in later stages of oogenesis requires adequate energy production and a high level of mitochondrial biogenesis²², so the mitochondrial abnormalities we observe in *RpS5b* ovaries may explain some aspects of their phenotype. Mitochondrial dysfunction has been previously linked by others to female infertility and failure of oogenesis, including in *Drosophila*²⁶.

In conclusion, our study provides further direct evidence that specialized ribosomes can play a pivotal physiological role in a metazoan. In yeast where many ribosomal proteins are encoded by paralog pairs, three specific paralogs (Rpl1b, Rpl2b, and Rps26b) are required for proper mitochondrial morphology and function²⁷. We therefore conclude that translational control through variant ribosomes is a well conserved regulatory mechanism that is particularly important for ensuring appropriate expression of nuclear genes encoding mitochondrial proteins.

Materials and Methods

Fly stocks. We used Oregon-R flies as wild-type controls. All other fly lines are from the Bloomington *Drosophila* Stock Center unless stated otherwise. The *RpS5b*^{G5346} mutant (Bloomington #30152) carries an EP-element insertion that disrupts the 5' UTR of both predicted transcripts of the *RpS5b* gene. *RpS5a*^{GL10502} (Bloomington #43160) carries a TRiP insertion that expresses shRNA targeting *RpS5a*²⁸. The driver flies were *nos*-Gal4:VP16 (gift of M. Fuller) and MTD-Gal4 (Bloomington #31777)²⁹. To generate the germline homozygous mutant clones, we used FRT(82B) (Bloomington #2035 and #2149) and a heat-shock FLP line (Bloomington #7). To generate transgenic flies, the open reading frame (ORF) of *RpS5a* or *RpS5b* was inserted into the pENTR vector (Life Technologies) and flipped into expression vectors pPFHW, pPVW and pPW from the *Drosophila* Gateway Vector collection. The final constructs were injected into a *y w* fly (Kyoto Stock Center, #101079) for random insertion. The transformants were double balanced on both the 2nd and 3rd chromosome (by crossing to the line #109551, Kyoto Stock Center).

Immunostaining. Immunostainings were carried out as described³⁰ with the following modifications. Ovaries were dissected from 5–10 day old female flies in PBST (PBS with 0.3% Triton-100) and fixed in PBST with 4% formaldehyde for 20 min at room temperature (RT). Fixed ovaries were washed at least 3 times with PBST, permeabilized in PBS with 1% Triton X-100 for 1 h, and blocked in PBSTA (PBST with 1% bovine serum albumin) for 1 h. Samples were incubated with primary antibodies overnight at 4 °C in PBSTA. The dilutions of the primary antibodies were as follows: α -RpS5b (peptide antibody generated by Biomatik) 1:1000; α -RpS5a (peptide antibody was generated by Biomatik) 1:1000; α - α -Tubulin (Sigma) 1:5000; α -Orb (DSHB) 1:50; α -Dhc (DSHB) 1:50; α -cleaved Caspase 3 (Abcam), 1:200; α -ATP5A (Abcam) 1:1000; α -Aub 1:1000; α -Osk 1:500; α -Grk 1:500. Antisera were produced in the Lasko lab unless otherwise noted. Venus-tagged proteins were imaged directly under ultraviolet light.

Samples were washed and incubated in the dark with fluorescent secondary antibody (preadsorbed goat anti-rabbit Alexa Fluor555, or goat anti-mouse Alexa Fluor488, Molecular Probes, 1:500) in PBSTA for 90 min at RT. Samples were then dark washed and counterstained with DAPI, mounted in 1% DABCO (in 90% glycerol) anti-fade reagent, and examined under confocal microscopy (Zeiss LSM510).

Immunoprecipitation and Western blot analysis. 20 μ l Dynabeads (Life Technologies) was conjugated to 2 μ g primary antibody in 100 μ l of PBS with 1% NP-40 for 30 min at RT. Ovaries were dissected in PBST, immediately transferred to ice and lysed in 50 mM HEPES, pH 7.5, 100 mM KCl, 12 mM MgCl₂, 1% NP-40, 1 mM dithiothreitol, 1x Halt protease inhibitor, RNaseOut RNase inhibitor and 100 μ g/mL cycloheximide (lysis/IP buffer) on ice. The lysate was centrifuged at 10,000 \times g for 15 min at 4 °C. Supernatant was transferred to the Ab-conjugated beads, and incubated on a rotator at 4 °C for 1.5 h. The beads were washed with lysis/IP buffer and eluted with 2x SDS loading buffer by boiling for 3 min at 95 °C. Protein samples were resolved on SDS-PAGE and probed with antibodies. Primary antibody concentrations used in Western blots were: α -RpS5a 1:1000; α -RpS5b 1:1000; α -RpS6 (Cell Signalling) 1:300; α - α -Tubulin 1:5000; α -pAbp 1:30,000; α -ND-30 1:1000; α -Porin (Abcam) 1:500.

Sucrose gradients. Lysates were prepared from wild-type ovaries and fractionated on 10–50% linear sucrose gradients. Fractions were run on an SDS-PAGE gel, immunoblotted, and incubated with antisera recognizing proteins as indicated. α -Tubulin was used as a control cytosolic protein.

Cell lysate fractionation and mitochondria purification. Mitochondria were purified as described³¹ with the following adaptations. Dissected ovaries were homogenized in mitochondria isolation buffer (250 mM sucrose, 10 mM Tris, pH 7.5, 1 mM EDTA, 1x Halt protease inhibitor). The crude lysate was centrifuged at 600 \times g for 7 min at 4 °C. The pellet was discarded and the supernatant was centrifuged at 10,000 \times g for 15 min at 4 °C. The supernatant was the cytoplasmic S10 fraction. The pellet containing mitochondria was washed and resuspended in 10 mM HEPES and solubilized by sonication.

RIPseq. Polysome immunoprecipitations were carried out as described³² with the following adaptations. 15 mg of ovaries were homogenized using a Dounce in 10% w/v polysome buffer (50 mM Tris, pH 7.5, 100 mM

KCl, 12 mM MgCl₂, 1% NP-40, 1 mM DTT, 1 mg/mL heparin, 200 U/mL RNaseOut RNase inhibitor, protease inhibitors and 100 µg/mL cycloheximide) and centrifuged at 10,000 rpm for 10 min. 50 µl protein A/G magnetic beads (Dynabeads, Invitrogen) were saturated with 5 µg BSA and 200 U/mL RNaseOut, and homogenates were pre-cleared on 20 µl of beads for 1 h at 4 °C. Lysates, beads and 5 µg of α-RpS5b, α-RpS5a or non-immune IgG antibodies were mixed and rotated for 3 h at 4 °C. The beads were then washed 5 times in high salt buffer (50 mM Tris pH 7.5, 300 mM KCl, 12 mM MgCl₂, 1% NP-40, 1 mM DTT, 100 µg/mL cycloheximide). 25% of the washed beads were saved for Western blot. The bound RNA was purified by addition of 2.5 volumes of RLT buffer (Qiagen) and extracted using an RNeasy Mini kit according to the manufacturer's instructions (Qiagen). RNA concentrations were measured with a Nanodrop (ThermoFisher) and quality was evaluated with a Bioanalyser (Agilent).

In silico analysis of RNA sequencing. Read quality was assessed using FastQC. Read alignment was executed using TopHat on the *Drosophila* BDGP5.78/dm3 genomes from Ensembl³³. Read count was obtained with featureCounts³⁴. Normalized count values and differential expression was computed with DESeq²³⁵. Longest isoform UTR and CDS lengths were obtained through the R biomart library³⁶. Motif enrichment was determined using HOMER³⁷.

Proteomics. Purified mitochondria and the cytoplasmic S10 were subjected to liquid chromatography–tandem MS (LC–MS/MS) (Proteomics core facility, IRIC). See figure legends for the details of data analysis.

TEM Imaging. Ovaries were dissected from 5–15 day old female flies, fixed in 2.5% (vol/vol) glutaraldehyde in 0.1 M sodium cacodylate buffer, pH 7.4, and incubated overnight at 4 °C. The samples were washed with sodium cacodylate buffer three times for 30 min, and then post-fixed in 0.1 M sodium cacodylate buffer containing 1% (wt/vol) OsO₄ and 1.5% (wt/vol) potassium ferrocyanide for 2 h at 4 °C and en bloc stained with 1% (wt/vol) aqueous uranyl acetate at 4 °C. Samples were dehydrated in five successive steps of acetone and water [30–90% (vol/vol)], each for 15 min at room temperature followed by 100% acetone (3 × 20 min). The samples were incubated with increasing concentrations [30–100% (vol/vol)] of low viscosity EPON 812 replacement (Mecalab Limited, Montreal, QC) and acetone over a period of 24 h, and then polymerized at 65 °C for 48 h. Ultrathin sections (70–100 nm) were cut from the resin blocks using a Leica Microsystems EM UC7 ultramicrotome (Leica Microsystems) with a Diatome diamond knife (Diatome Ltd, Nidau, Switzerland). The sections were transferred onto 200-mesh Cu TEM grids (EMS, Hatfield, PA) and post-stained with 4% (wt/vol) aqueous uranyl acetate for 8 min followed with Reynold's lead for 5 min. Sections were imaged with an FEI Tecnai 12 TEM (Thermo Fisher Scientific, Hillsboro, OR) equipped with an AMT XR80C CCD camera (Advanced Microscopy Techniques, Woburn, MA) at an accelerating voltage of 120 kV in bright-field mode.

Serial block face imaging. Sample blocks for 3D characterization by FIB-SEM were prepared as described above for TEM. The blocks were trimmed with a razor blade to expose the region of interest (ROI), mounted on fixed 45° pre-tilt SEM stubs and coated with a 2 nm layer of platinum using a Leica Microsystems EM ACE600 sputter coater (Leica Microsystems) to enhance electrical conductivity. Milling of serial sections and imaging of the block face after each z-slice was carried out with the Helios Nanolab 660 DualBeam using Auto Slice & View G3 ver 1.2 software (Thermo Fisher Scientific). The sample block was first imaged to determine the orientation of the block face and ion and electron beams. A 2 µm layer of platinum was deposited on the surface of the ROI to protect the resin volume from ion beam damage and to correct for stage and/or specimen drift, i.e. orthogonal to the block face of the volume to be milled. Trenches on both sides of the ROI were created to minimize re-deposition during automated milling and imaging. Fiducials were generated for both ion and electron beam imaging and used to dynamically correct for drift in the x- and y-directions during data collection by applying appropriate SEM beam shifts. Milling was carried out at 30 kV with an ion beam current of 2.5 nA, stage tilt of 4°, and working distance of 4 mm.

At each step, a 4-nm slice of the block face was removed by the ion beam. Each newly milled block face was imaged with the in-column detector (ICD) at an accelerating voltage of 2 kV, beam current of 0.4 nA, stage tilt of 42°, and working distance of 2.5 mm. The pixel resolution was 3.9 nm with a dwell time of 30 µs per pixel. Pixel dimensions of the recorded image were 3072 × 2048 pixels. Three hundred fifty images were collected and the image contrast inverted. Visualization and direct 3-D volume rendering of the acquired datasets was performed with Amira for Life Sciences software (Thermo Fisher Scientific) with 100 successive images selected based on the ROI, i.e., mitochondria.

References

- Kong, J. & Lasko, P. Translational control in cellular and developmental processes. *Nat. Rev. Genet.* **13**, 383–394 (2012).
- Xue, S. & Barna, M. Specialized ribosomes: a new frontier in gene regulation and organismal biology. *Nat. Rev. Mol. Cell Biol.* **13**, 355–369 (2012).
- Buszczak, M., Signer, R. A. J. & Morrison, S. J. Cellular differences in protein synthesis regulate tissue homeostasis. *Cell* **159**, 242–251 (2014).
- Dinman, J. D. Pathways to specialized ribosomes: the Brussels lecture. *J. Mol. Biol.* **428**(10 Pt B), 2186–2194 (2016).
- Guo, H. Specialized ribosomes and the control of translation. *Biochem. Soc. Trans.* **46**, 855–869 (2018).
- Genuth, N. R. & Barna, M. The discovery of ribosome heterogeneity and its implications for gene regulation and organismal life. *Mol. Cell* **71**, 364–374 (2018).
- Komili, S., Farny, N. G., Roth, F. P. & Silver, P. A. Functional specificity among ribosomal proteins regulates gene expression. *Cell* **131**, 557–571 (2007).
- Zhang, Y. *et al.* Control of hematopoietic stem cell emergence by antagonistic functions of ribosomal protein paralogs. *Dev. Cell* **24**, 411–425 (2013).

9. Kondrashov, N. *et al.* Ribosome-mediated specificity in Hox mRNA translation and vertebrate tissue patterning. *Cell* **145**, 383–397 (2011).
10. Wang, R. *et al.* Loss of function mutations in RPL27 and RPS27 identified by whole-exome sequencing in Diamond-Blackfan anemia. *Br. J. Haematol.* **168**, 854–864 (2015).
11. Shi, Z. *et al.* Heterogeneous ribosomes preferentially translate distinct subpools of mRNAs genome-wide. *Mol. Cell* **67**, 71–83 (2017).
12. Marygold, S. J. *et al.* The ribosomal protein genes and Minute loci of *Drosophila melanogaster*. *Genome Biol.* **8**, R216 (2007).
13. Kearse, M. G., Chen, A. S. & Ware, V. C. Expression of ribosomal protein L22e family members in *Drosophila melanogaster*: rpL22-like is differentially expressed and alternatively spliced. *Nucleic Acids Res.* **39**, 2701–2716 (2011).
14. Graveley, B. R. *et al.* The developmental transcriptome of *Drosophila melanogaster*. *Nature* **471**, 473–479 (2011).
15. Kai, T., Williams, D. & Spradling, A. C. The expression profile of purified *Drosophila* germline stem cells. *Dev. Biol.* **283**, 486–502 (2005).
16. Shigenobu, S., Kitadate, Y., Noda, C. & Kobayashi, S. Molecular characterization of embryonic gonads by gene expression profiling in *Drosophila melanogaster*. *Proc. Natl. Acad. Sci. USA* **103**, 13728–13733 (2006).
17. Janic, A., Mendizabal, L., Llamazares, S., Rossell, D. & Gonzalez, C. Ectopic expression of germline genes drives malignant brain tumor growth in *Drosophila*. *Science* **330**, 1824–1827 (2010).
18. McKim, K. S., Dahmus, J. B. & Hawley, R. S. Cloning of the *Drosophila melanogaster* meiotic recombination gene mei-218: a genetic and molecular analysis of interval 15E. *Genetics* **144**, 215–228 (1996).
19. Bellen, H. J. *et al.* The *Drosophila* gene disruption project: progress using transposons with different site specificities. *Genetics* **188**, 731–743 (2011).
20. Chou, T. B. & Perrimon, N. The autosomal FLP-DFS technique for generating germline mosaics in *Drosophila melanogaster*. *Genetics* **144**, 1673–1679 (1996).
21. Sun, J. J. & Deng, W.-M. Notch-dependent downregulation of the homeodomain gene cut is required for the mitotic cycle/endocycle switch and cell differentiation in *Drosophila* follicle cells. *Development* **132**, 4299–4308 (2005).
22. Zhang, Y., Chen, Y., Gucek, M. & Xu, H. The mitochondrial outer membrane protein MDI promotes local protein synthesis and mtDNA replication. *EMBO J.* **35**, 1045–1057 (2016).
23. Ghosh, S. & Lasko, P. Loss-of-function analysis reveals distinct requirements of the translation initiation factors eIF4E, eIF4E-3, eIF4G, and eIF4G2 in *Drosophila* spermatogenesis. *PLoS ONE* **10**(4), e0122519 (2015).
24. Hernández, G. *et al.* Mextli is a novel eukaryotic translation initiation factor 4E-binding protein that promotes translation in *Drosophila melanogaster*. *Mol. Cell. Biol.* **33**, 2854–2864 (2013).
25. Lopes, A. M. *et al.* The human RPS4 paralogue on Yq11.223 encodes a structurally conserved ribosomal protein and is preferentially expressed during spermatogenesis. *BMC Mol. Biol.* **11**, 33 (2010).
26. Zhang, C., Montooth, K. L. & Calvi, B. Incompatibility between mitochondrial and nuclear genomes during oogenesis results in ovarian failure and embryonic lethality. *Development* **144**, 2490–2503 (2017).
27. Segev, N. & Gerst, J. E. Specialized ribosomes and specific ribosomal protein paralogs control translation of mitochondrial proteins. *J. Cell Biol.* **217**, 117–126 (2018).
28. Ni, J. Q. *et al.* A genome-scale shRNA resource for transgenic RNAi in *Drosophila*. *Nat. Methods* **8**, 405–407 (2011).
29. Rorth, P. Gal4 in the *Drosophila* female germline. *Mech. Dev.* **78**, 113–118 (1998).
30. Hawkins, N. C., Van Buskirk, C., Grossniklaus, U. & Schüpbach, T. Post-transcriptional regulation of germline by encore is required for axis determination in *Drosophila*. *Development* **124**, 4801–4810 (1997).
31. Antonicka, H. & Shoubridge, E. A. Mitochondrial RNA granules are centers for posttranscriptional RNA processing and ribosome biogenesis. *Cell Rep.* **10**, 920–932 (2015).
32. Sanz, E. *et al.* Cell-type-specific isolation of ribosome-associated mRNA from complex tissues. *Proc. Natl. Acad. Sci. USA* **106**, 13939–13944 (2009).
33. Trapnell, C. *et al.* Differential gene and transcript expression analysis of RNA-seq experiments with TopHat and Cufflinks. *Nat. Protoc.* **7**, 562–578 (2012).
34. Liao, Y., Smyth, G. K. & Shi, W. featureCounts: an efficient general purpose program for assigning sequence reads to genomic features. *Bioinformatics* **30**, 923–930 (2014).
35. Anders, S. & Huber, W. Differential expression analysis for sequence count data. *Genome Biol.* **11**(10), R106 (2010).
36. Durinck, S., Spellman, P. T., Birney, E. & Huber, W. Mapping identifiers for the integration of genomic datasets with the R/Bioconductor package biomaRt. *Nat. Protoc.* **4**, 1184–1191 (2009).
37. Heinz, S. *et al.* Simple combinations of lineage-determining transcription factors prime cis-regulatory elements required for macrophage and B cell identities. *Mol. Cell* **38**, 576–589 (2010).
38. Love, M., Anders, S. & Huber, M. Differential gene expression analysis based on the negative binomial distribution. *Genome Biol.* **15**, 550 (2014).
39. Mi, H. *et al.* PANTHER version 11: expanded annotation data from Gene Ontology and Reactome pathways, and data analysis tool enhancements. *Nucleic Acids Res.* **45**, D183–D189 (2017).

Acknowledgements

We are grateful to Hana Antonicka and Eric Shoubridge for helpful discussions and assistance with mitochondrial fractionations. This work was supported by CIHR grants MOP-44050 and IOP-107945 to P. L. J. B. was supported by a FRQ-S postdoctoral scholarship, E. L. is a Junior 2 FRQ-S Scholar. Work in the Lécuyer lab is supported by an FRQ-S strategic team grant and by CIHR grant MOP-137096.

Author Contributions

J. Kong, H. Han, J. Bergalet and G. Hernández performed the experiments, L.P.B. Bouvrette analyzed RNA sequencing and mass spectrometry data, N. Moon, H. Vali, G. Hernández, E. Lécuyer, and P. Lasko analyzed experimental data, E. Lécuyer and P. Lasko designed experiments, J. Kong, E. Lécuyer and P. Lasko prepared the manuscript.

Additional Information

Supplementary information accompanies this paper at <https://doi.org/10.1038/s41598-019-50357-z>.

Competing Interests: The authors declare no competing interests.

Publisher's note Springer Nature remains neutral with regard to jurisdictional claims in published maps and institutional affiliations.



Open Access This article is licensed under a Creative Commons Attribution 4.0 International License, which permits use, sharing, adaptation, distribution and reproduction in any medium or format, as long as you give appropriate credit to the original author(s) and the source, provide a link to the Creative Commons license, and indicate if changes were made. The images or other third party material in this article are included in the article's Creative Commons license, unless indicated otherwise in a credit line to the material. If material is not included in the article's Creative Commons license and your intended use is not permitted by statutory regulation or exceeds the permitted use, you will need to obtain permission directly from the copyright holder. To view a copy of this license, visit <http://creativecommons.org/licenses/by/4.0/>.

© The Author(s) 2019